# Density Functional Theory Calculations of the Non-Resonant and Resonant X-ray Emission Spectroscopy of Carbon Fullerenes and Nanotubes

Magnus W. D. Hanson-Heine,[a] Michael W. George[a,b] and Nicholas A. Besley[a]*

[a] *School of Chemistry, University of Nottingham, University Park, Nottingham, NG7 2RD, UK,* [b] *Department of Chemical and Environmental Engineering, University of Nottingham Ningbo China, 199 Taiking East Rd., Ningbo 315100, Zhejiang, China.*

**Abstract**

The non-resonant X-ray emission spectroscopy of fullerenes and carbon nanotubes is studied with density functional theory in conjunction with short-range corrected functionals. For $C_{60}$ and $C_{70}$ the X-ray emission spectra are insensitive to modest structural changes, and absorption onto the fullerene cage has the greatest effect with a broader less structured band observed with the high energy $\pi$ band reduced in intensity. For carbon nanotubes the X-ray emission spectra are shown to be weakly dependent on the length and chirality of the nanotube. However, some variation with the diameter of the tube is observed in both resonant and non-resonant spectra.

*Keywords:* X-ray emission spectroscopy, fullerenes, carbon nanotubes, density functional theory

## 1. Introduction

The increasing availability of synchrotron sources and free-electron lasers has led to spectroscopic techniques in the X-ray region being applied in a wide range of research areas [1–4]. One advantage of these techniques compared with other spectroscopic methods is that they are element specific and can provide a local probe of structure. More recently, these techniques have been used to

[1] nick.besley@nottingham.ac.uk (Nicholas Besley)

study ultrafast chemical processes through time-resolved measurements [5–7]. There are several commonly used spectroscopic techniques in the X-ray region which can provide complementary information. For example, X-ray emission spectroscopy (XES) probes the occupied orbitals while X-ray absorption spectroscopy (XAS) probes the unoccupied orbitals. Resonant inelastic X-ray scattering (RIXS) represents an extension of XES wherein the intermediate state is a core-excited state rather than the core-ionised state in XES. Simulations of X-ray spectroscopy can play an important role in interpreting and understanding spectra measured by experiment. Within the framework of density functional theory (DFT), X-ray absorption spectra are commonly simulated using either transition-potential or time-dependent density functional theory (TDDFT) approaches [8, 9]. Accurate core-excitation energies can be obtained from TDDFT calculations with the use of short-range corrected (SRC) functionals [10] and it has been shown how these calculations can be applied to study large systems [11].

There has been less focus on the calculation of XES, one approach is to apply TDDFT or equation of motion coupled cluster theory to a reference determinant describing the core-ionised state [12], and these approaches have been applied to study the XES of organic [13] and inorganic [14, 15] molecules. Alternatively, X-ray emission spectra can be determined directly from a Kohn-Sham DFT calculation. In this approach the transition energy is evaluated from the orbital energies of the valence orbital ($\epsilon_v$) and core orbital ($\epsilon_c$)

$$\Delta E = \epsilon_v - \epsilon_c \; . \tag{1}$$

The associated intensity can be determined from the following transition matrix element

$$f \propto |\langle \phi_c | \hat{\mu} | \phi_v \rangle|^2 \tag{2}$$

where a valence orbital ($\phi_v$) is taken to be the initial state and the final state is a core orbital ($\phi_c$). Recently, it has been shown that this approach can provide

accurate X-ray emission spectra when the DFT calculation is performed with a SRC exchange-correlation functional [16]. These functionals were introduced for the calculation of X-ray absorption spectra and incorporate an increased fraction of Hartree-Fock exchange in the short range (low $r_{12}$) in the evaluation of the exchange energy contribution. It was demonstrated that this approach could be extended to simulate RIXS in a two-step procedure where a reference determinant describing the intermediate core-excited state is used in the Kohn-Sham DFT calculation. Although it was necessary to average over a number of structures from a molecular dynamics (MD) simulation in the core-excited state to achieve a reasonable agreement with experiment. The importance of including vibrations via molecular dynamics sampling has also been observed in earlier work [17]. The advantage of these approaches is that determining the XES spectra adds no significant computation cost relative to the cost of the Kohn-Sham DFT calculation, allowing large systems to be studied.

Carbon nanomaterials, including fullerenes and carbon nanotubes (CNT), have been the focus of considerable interest owing to their unique structural, mechanical and electronic properties. Spectroscopic methods are often used to characterise the structure of these materials. For example, Raman spectroscopy can provide information on the structure, bonding and environment of CNTs [18] and graphene [19], including details on CNT diameter, chirality and defects. One key mode is the radial breathing mode and the frequency of this mode is known to depend on the diameter of the CNT. A further band is the disorder-induced D band, which is associated with $sp^3$ defects in CNTs [20]. CNTs can also be studied using fluorescence [21] and nuclear magnetic resonance spectroscopies [22, 23], and there has been a considerable effort focused on accurate simulations of the spectroscopy of these systems, for examples see references [24–30]. Spectroscopic studies have also shown that hydrogenation of fullerenes has a significant effect on its electronic structure. The ability to tune the photophysical properties of $C_{60}H_x$ has potential applications in a range of devices where carbon based materials have a number of advantages compared

to commonly used transition metal based quantum dot chromophores [31].

Carbon nanomaterials have also been studied with X-ray spectroscopy. Kawai and Motoyama reported X-ray emission spectra for solid $C_{60}$ and $C_{70}$ [32]. The experimental spectra were compared with spectra simulated from the 2p density of states from a Hartree-Fock theory calculation. The X-ray emission spectrum of $C_{60}$ has also been measured and calculated by Heggie and co-workers [33]. The core-hole was treated as a nitrogen impurity in the Z+1 approximation and the spectrum simulated from the p-projected density of occupied states. The calculations reproduced the bands observed in experiment. Other fullerenes have also been studied, for example the X-ray emission spectra of different isomers of $C_{82}$ have been calculated [34] and the X-ray emission spectrum of bulk $K_3C_{60}$ measured [35]. The XES of hydrofullerene ($C_{60}H_{36}$) [36] and fullerene fluoride ($C_{60}F_{24}$) [37] has been studied. For both of these molecules, the distinct bands present in the X-ray emission spectrum of $C_{60}$ are not evident and only a broad peak is observed. RIXS spectra have been reported for $C_{60}$ and $C_{70}$ [38, 39]. For $C_{60}$ there is a significant variation between the spectra excited at different photon energies.

X-ray emission spectra for nanotubes have also been reported [40–42]. In one study [40] four peaks were identified and spectra simulated based upon semi-empirical PM3 calculations using finite nanotube structures with the end carbons capped with hydrogen atoms. Only small differences between the spectra for zigzag and armchair nanotubes were observed. X-ray emission spectra of multi-walled nanotubes showed a small contraction in the high energy region of the spectrum with decreasing diameter [41]. Resonant X-ray emission spectra showed a strong dependence on the diameter of the tubes at an excitation energy of 285.5 eV, corresponding to a core$\rightarrow \pi^*$ excitation [43]. It was suggested that this might provide a technique to determine the mean tube diameter. In this paper DFT calculations are used to study the X-ray emission spectra of carbon fullerenes and nanotubes and study the sensitivity of the spectra to modifica-

tions of the structure. Subsequently, the extension of the calculations to study the RIXS spectra of these materials is explored.

## 2. Computational Details

The structure of the fullerenes and nanotubes were optimised at the B3LYP/6-31G* level of theory [44, 45]. The nanotube calculations used finite length nanotubes with enclosed (capped) ends, similar to those used in previous work [25]. X-ray emission spectra were computed according to equations 1 and 2 from a Kohn-Sham DFT calculation using the short-range corrected SRC1r1 exchange-correlation functional [10]. Details of the methodology underlying the calculations have been described fully elsewhere [16], and a more brief account is given here. In the SRC1r1 functional, the electron repulsion operator is partitioned according to

$$\begin{aligned} \frac{1}{r_{12}} &\equiv C_{\mathrm{SHF}}\frac{\mathrm{erfc}(\mu_{\mathrm{SR}}r_{12})}{r_{12}} - C_{\mathrm{SHF}}\frac{\mathrm{erfc}(\mu_{\mathrm{SR}}r_{12})}{r_{12}} \\ &+ C_{\mathrm{LHF}}\frac{\mathrm{erf}(\mu_{\mathrm{LR}}r_{12})}{r_{12}} - C_{\mathrm{LHF}}\frac{\mathrm{erf}(\mu_{\mathrm{LR}}r_{12})}{r_{12}} + \frac{1}{r_{12}} \end{aligned} \tag{3}$$

The first and third terms of equation 3 are treated with HF exchange and DFT exchange used for the remaining terms. The four parameters in the functional, $C_{\mathrm{SHF}}$, $C_{\mathrm{LHF}}$, $\mu_{\mathrm{SR}}$ and $\mu_{\mathrm{LR}}$, determine the amount of Hartree-Fock exchange in the short and long range, and these parameters were optimised to reproduce a set of core-excitation energies [10]. Two sets of parameters were optimised, the first for excitations at the K-edge of first row nuclei and the second for excitations from second row nuclei, and these functionals are denoted SRC1r1 and SRC1r2, respectively. These functionals correct the orbital energy of the core orbitals and result in more accurate transitions energies for X-ray emission when evaluated from the different in the orbital energies. In the evaluation of the transition matrix elements to determine the intensity, the final and initial states are approximated by the valence and core molecular orbitals associated with the transition (see equation 2).

The 6-31G* basis set was also used for the calculations of the X-ray emission spectra. For $C_{60}$, there is little difference between the spectrum computed with this basis set and spectrum computed using the larger 6-311G* basis set except that the spectrum for the 6-31G* is about 0.4 eV higher in energy. A comparison between these two calculated spectra is shown in the Supplementary Content. However, the small size of this basis set allows larger systems to be studied more readily. Spectra were generated by convoluting the transitions with Lorentzian functions with a width of 1 eV. All calculations were performed with the Q-CHEM software package [46].

A RIXS spectrum for $C_{60}$ was computed using a similar approach but with a reference determinant corresponding to a core to lowest unoccupied molecular orbital (LUMO) excited state. $C_{60}$ has three degenerate LUMOs, however, the resulting spectrum does not depend on which of these are occupied. The core excited state is maintained during the self-consistent field calculation by using the maximum overlap method [47]. The B3LYP functional in conjunction with the 6-31G* basis set was used for these calculations as suggested by previous work [16]. A spectrum is also computed by averaging over 100 structures taken from an ab initio molecular dynamics simulation for the excited state. These structures were sampled at equal time intervals from a 24 femtosecond simulation at 300 K.

## 3. Results and Discussion

Figure 1 shows the computed and experimental non-resonant X-ray emission spectra for $C_{60}$ and $C_{70}$. For both $C_{60}$ and $C_{70}$ the calculations reproduce the shape of the experimental spectra well, although the calculations predict the transition energies to be too high, and the calculated spectra need to be shifted by -1.4 eV to align with experiment. The spectra have been decomposed into contributions from $\sigma$ and $\pi$ orbitals. The most intense bands in the spectra correspond to transitions from $\sigma$ orbitals, while the high energy bands at 281.7 eV

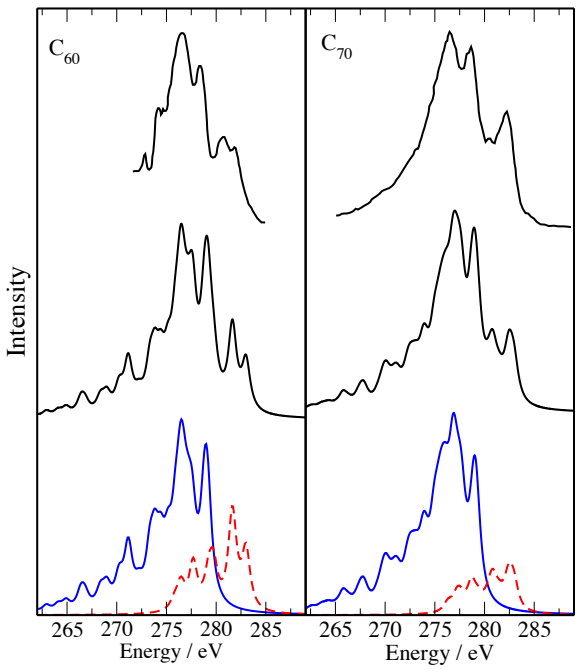


Figure 1: Calculated and experimental non-resonant X-ray emission spectra for $C_{60}$ and $C_{70}$. Upper spectra: experiment, adapted from references [36, 38]. Middle spectra: Calculated SRC1r1/6-31G* spectra. Lower spectra: Calculated spectra decomposed into contributions from $\sigma$ orbitals (solid blue line) and $\pi$ orbitals (dashed red line).

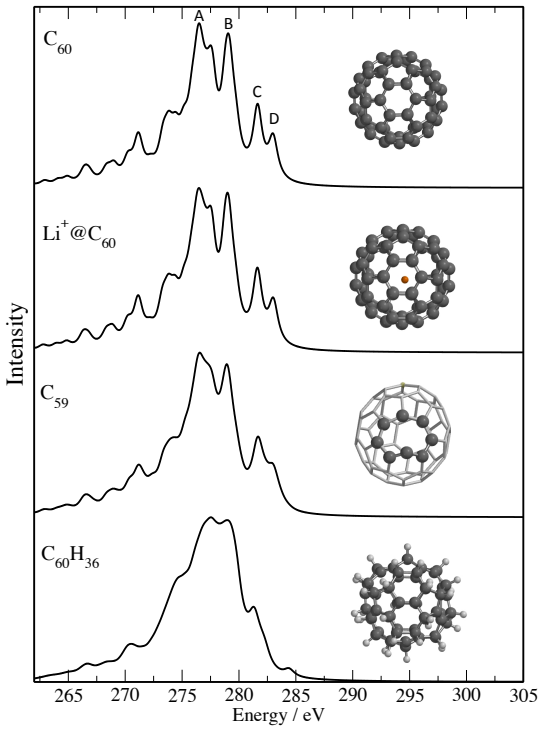


Figure 2: Calculated SRC1r1/6-31G* non-resonant X-ray emission spectra for modified $C_{60}$, including encapsulated $Li^+$, vacancy defect and hydrofullerene.

and 283.0 eV in $C_{60}$, and 280.8 eV and 282.7 eV in $C_{70}$ arise from $\pi$ orbitals. In general the two molecules have similar spectra. One noticeable difference is the relative intensity of the two high energy bands associated with the $\pi$ orbitals. The calculations show that the lower energy band is more intense, while for $C_{70}$ the intensities are similar. This feature is also evident in the experimental spectra.

In order to explore the sensitivity of the X-ray emission spectra to structural modifications of the fullerene cage, Figure 2 shows computed spectra for $C_{60}$ with an encapsulated $Li^+$ ion, a vacancy defect and with adsorbed hydro-

gen atoms (hydrofullerene $C_{60}H_{36}$). For each system the structure has been re-optimised and for $C_{59}$ the ground state is a triplet state. Encapsulation of $Li^+$ results in no observable affect on the computed X-ray emission spectrum. The vacancy defect leads to some minor changes in the spectrum, particularly in the $\pi$ bands (C and D). However, changes of this magnitude are likely to be too small to be distinguished reliably in experiment. The greatest change is observed for hydrofullerene, and the spectrum has fewer distinct features. The bands A and B have merged, and the band D, arising from $\pi$ orbitals, is greatly diminished. This is not surprising since many of the carbons are now $sp^3$ carbons, and with further saturation of the fullerene cage the intensity of this band would be expected to be reduced further. The band corresponding to C in the spectrum does arise from an orbital that has $\pi$ character, but this orbital also has C-H $\sigma$ character. These findings are consistent with the experimental spectrum for $C_{60}H_{36}$ [36]. Based upon the systems studied here, the X-ray emission spectra of fullerenes are insensitive to modest structural changes. Absorption onto the fullerene cage has the greatest effect with a broader less structured band observed and the high energy $\pi$ band reduced in intensity.

Figure 3 shows the computed RIXS spectrum. The Kohn-Sham calculation for the core-excited state results in an unoccupied orbital that is localised on one of the carbon atoms. The resulting spectrum is significantly different from the non-resonant spectrum, however, there are some notable similarities. The most intense bands arise from transitions from $\sigma$ orbitals while the high energy bands correspond to transitions from $\pi$ orbitals. In the case of $C_{60}$ studied here, incorporating vibrational coupling through averaging over structures from a molecular dynamics simulation has little effect on the resulting spectrum. For the RIXS spectrum, the agreement with the available experimental data is not as good as for the non-resonant spectrum. The computed spectrum is closest to the spectrum at an excitation energy of 283.9 eV which corresponds to the rising edge of the intense core$\rightarrow \pi^*$ band [39]. We note that the simulation of the RIXS spectrum may be improved through the use of the Kramers-Heisenberg

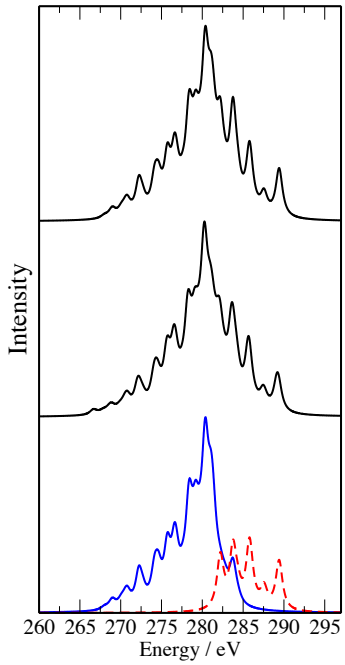


Figure 3: Calculated resonant X-ray emission (RIXS) spectra of $C_{60}$. Upper spectrum: Calculated SRC1r1/6-31G* spectrum for the optimised ground state structure. Middle spectrum: Calculated SRC1r1/6-31G* spectrum averaged over 100 structures from an ab initio molecular dynamics simulation. Lower spectrum: Calculated spectra decomposed into contributions from $\sigma$ orbitals (solid blue line) and $\pi$ orbitals (dashed red line).

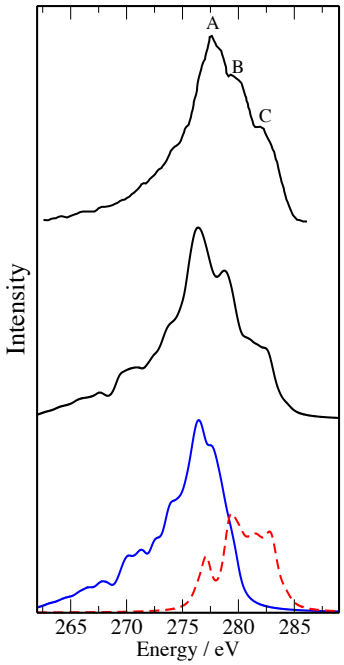


Figure 4: Calculated and experimental non-resonant X-ray emission spectra for a model (9,0) nanotube of length 30 Å. Upper spectrum: experiment, adapted from reference [41]. Middle spectrum: Calculated SRC1r1/6-31G* spectrum. Lower spectrum: Calculated spectrum decomposed into contributions from $\sigma$ orbitals (solid blue line) and $\pi$ orbitals (dashed red line).

approach [48, 49], however, such an approach is currently beyond our current capabilities for a system the size of $C_{60}$.

The accuracy of the calculated non-resonant X-ray emission spectra for $C_{60}$ and $C_{70}$ provides some confidence that the methodology can be applied to carbon nanotubes. The calculated spectrum for a (9,0) nanotube of length 30 Å is shown in Figure 4 with an experimental spectrum available in the literature [41]. The computed spectrum has been shifted by the value of -1.4 eV determined for $C_{60}$. Despite differences in the nature of the tubes in the measured sample and

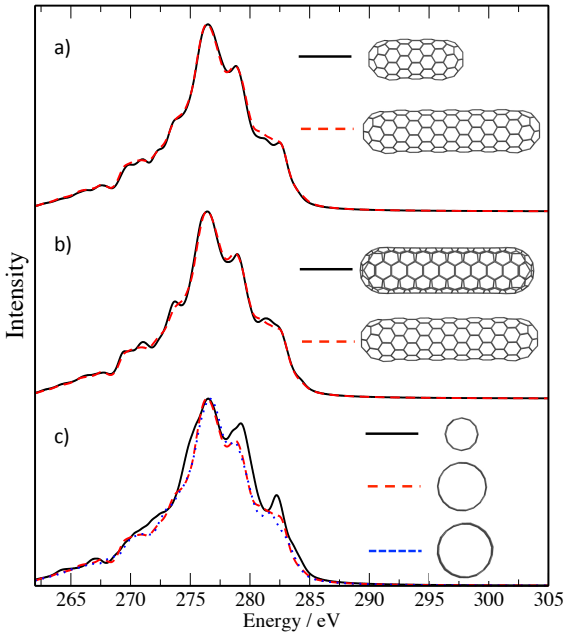


Figure 5: Calculated SRC1r1/6-31G* non-resonant X-ray emission spectra for different nanotubes. a) (9,0) nanotubes of length 17 Å and 30 Å, b) (9,0) and (5,5) nanotubes and c) (6,0), (9,0) and (10,0) nanotubes.

the (9,0) tube used in the calculations, the computed spectrum reproduces the features observed in experiment accurately. The calculations show that peak A arises from $\sigma$-type orbitals while bands B and C correspond to orbitals of $\pi$ character.

Figure 5 shows the variation in the computed X-ray emission spectra to the structure of the nanotube. The calculations show that lengthening the (9,0) tube from 17 Å to 30 Å has only a minor effect on the spectrum. Similarly, changing the chirality of the nanotunbe from zigzag to armchair also does not change the spectrum. For both of these, there is a small change for the $\pi$ orbital bands. The spectra showing the variation in diameter for (6,0), (9,0) and (10,0)

nanotubes show that there is greater sensitivity to the diameter. Exploring the variation in the spectra with diameter is limited to relativity narrow tubes when using capped nanotube models. The diameters of the (6,0), (9,0) and (10,0) nanotubes are 5.0 Å, 7.0 Å and 8.0 Å, respectively. Since the length of the nanotube is not a crucial factor, we have investigated the variation of the spectra with diameter using short fragments of nanotube capped with hydrogen atoms. The structure of these fragments were produced from a nanotube generator with a carbon-carbon bond length of 1.421 Å. For these spectra, only transitions to the core orbitals of the carbon atoms of the inner rings are included. Including only these central carbons has the effect of excluding effects arising from hydrogenation and also to minimise any effects the length of the fragments.

The diameters of the hydrogen-capped tubes studied are significantly larger, with the (24,0) nanotube having a diameter of about 18.8 Å. For the non-resonant X-ray emission spectra, the main change in the spectra is at about 285 eV (Figure 6) with the bands associated predominantly with transitions from $\pi$-like orbitals. For this band there is a relative reduction in the intensity as the diameter of the nanotube increases. There is also a noticeable change in the intensity at about 280 eV. Experimental studies have shown a dependence of the intensity on the diameter of the nanotube in RIXS measurements [43]. Computing non-resonant X-ray emission spectra for these nanotube models is challenging, and the method used for $C_{60}$ where the core-excited state is considered with the Kohn-Sham calculation proved problematic to converge. Consequently, we have adopted a more crude approach to estimate the RIXS spectra of these systems. In this approach one carbon atom is replaced by a nitrogen atom and a calculation performed on the resulting doublet state. The rationale for this approach is that the additional electron occupied the LUMO and the nitrogen nuclei represents a carbon nuclei with a core-hole. This is similar to the scheme used elsewhere to calculate non-resonant X-ray emission of $C_{60}$ [33]. The predicted excitation energies are too high, however, in the case

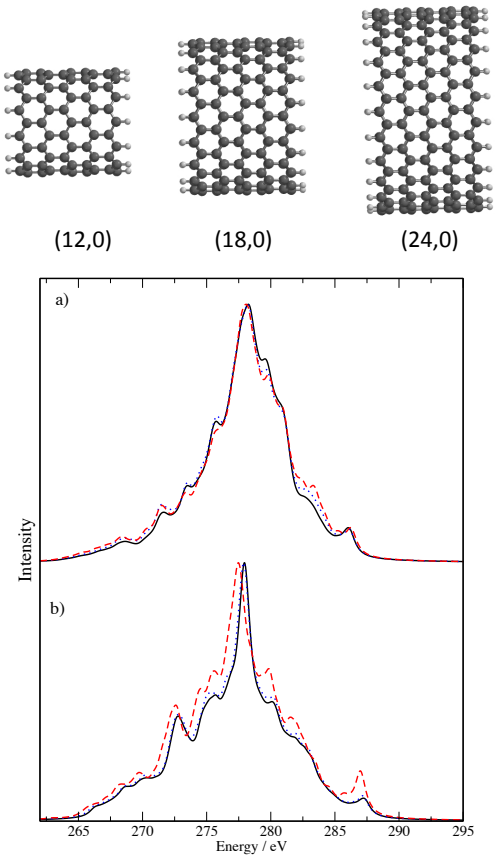


Figure 6: Calculated non-resonant (a) and resonant (b) X-ray spectra for finite hydrogen-capped nanotubes with different diameters. (24,0): solid black line, (18,0): dotted blue line and (12,0): dashed red line.

of $C_{60}$ the resulting spectrum has a similar shape to the spectrum computed with a core-hole. The resulting spectra for nanotubes using this approach are also shown in Figure 6. These spectra have been shifted by -102.05 eV so that the maximum aligns with the non-resonant spectra. The calculated spectra do show a reduction in the intensity of the peaks either side of the most intense band as the diameter of the tube increases. This trend does match observations from experiment [43] but the magnitude of the changes in the calculations is much smaller.

## 4. Conclusions

The calculation of the non-resonant and resonant X-ray emission spectra of carbon fullerenes and nanotubes using DFT has been investigated. Non-resonant X-ray emission spectra can be computed accurately with short-range corrected exchange-correlation functionals and modest sized basis sets. The spectrum for $C_{60}$ did not show significant changes on encapsulation of a $Li^+$ ion or the presence of a vacancy defect. Absorption of hydrogen (hydrofullerene) gave a broad, less structured band with a reduction in intensity of the high energy bands associated with $\pi$ orbitals. Similarly, for nanotubes the non-resonant spectra were insensitive to changes in length and chirality but did show some dependence on the diameter of the nanotubes. Simulating the resonant X-ray emission spectra (RIXS) is more challenging and the agreement with experiment is poorer. Two approaches have been used, one involving explicit consideration of the core-excited state and a simpler scheme where a carbon atom is substituted with nitrogen. The calculations show that for $C_{60}$ the most intense bands arise from transitions from $\sigma$ orbitals, with higher nervy bands corresponding to $\pi$ orbitals. Inclusion of vibrational coupling through sampling structures from an ab initio molecular dynamics simulation had little effect on the resulting spectrum compared with the spectrum for the optimised ground state structure. For nanotubes. the calculations indicate some dependence on the diameter of the nanotube in non-resonant spectra.

**Acknowledgements**

This work was supported by the Engineering and Physical Sciences Research Council [Grant No. EP/N002148/1]. The authors would like to thank the University of Nottingham for access to its High Performance Computing facility.

**Appendix A. Supplementary material**

Supplementary data associated with this article can be found, in the online version, at

**References**

[1] J. Chen, NEXAFS investigations of transition metal oxides, nitrides, carbides, sulfides and other interstitial compounds, Surf. Sci. Rep. 30 (1997) 1 – 152.

[2] A. Nilsson, L. G. M. Pettersson, Chemical bonding on surfaces probed by X-ray emission spectroscopy and density functional theory, Surf. Sci. Rep. 55 (2004) 49 – 167.

[3] P. Glatzel, U. Bergmann, High resolution 1s core hole X-ray spectroscopy in 3d transition metal complexes electronic and structural information, Coord. Chem. Rev. 249 (2005) 65 – 95.

[4] T. Fransson, Y. Harada, N. Kosugi, N. A. Besley, B. Winter, J. J. Rehr, L. G. M. Pettersson, A. Nilsson, X-ray and electron spectroscopy of water, Chem. Rev. 116 (2016) 7551–7569.

[5] M. Dell'Angela, T. Anniyev, M. Beye, R. Coffee, A. Föhlisch, J. Gladh, T. Katayama, S. Kaya, O. Krupin, J. LaRue, A. Møgelhøj, D. Nordlund, J. K. Nørskov, H. Öberg, H. Ogasawara, H. Öström, L. G. M. Pettersson, W. F. Schlotter, J. A. Sellberg, F. Sorgenfrei, J. J. Turner, M. Wolf, W. Wurth, A. Nilsson, Real-time observation of surface bond breaking with an X-ray laser, Science 339 (2013) 1302–1305.

[6] H. Öström, H. Öberg, H. Xin, J. LaRue, M. Beye, M. Dell'Angela, J. Gladh, M. L. Ng, J. A. Sellberg, S. Kaya, G. Mercurio, D. Nordlund, M. Hantschmann, F. Hieke, D. Kühn, W. F. Schlotter, G. L. Dakovski, J. J. Turner, M. P. Minitti, A. Mitra, S. P. Moeller, A. Föhlisch, M. Wolf, W. Wurth, M. Persson, J. K. Nørskov, F. Abild-Pedersen, H. Ogasawara, L. G. M. Pettersson, A. Nilsson, Probing the transition state region in catalytic CO oxidation on Ru, Science 347 (2015) 978–982.

[7] P. Wernet, K. Kunnus, I. Josefsson, I. Rajkovic, W. Quevedo, M. Beye, S. Schreck, S. Grubel, M. Scholz, D. Nordlund, W. Zhang, R. W. Hartsock, W. F. Schlotter, J. J. Turner, B. Kennedy, F. Hennies, F. M. F. de Groot, K. J. Gaffney, S. Techert, M. Odelius, A. Fohlisch, Orbital-specific mapping of the ligand exchange dynamics of $Fe(CO)_5$ in solution, Nature 520 (2015) 78–81.

[8] L. Triguero, L. G. M. Pettersson, H. Ågren, Calculations of near-edge x-ray-absorption spectra of gas-phase and chemisorbed molecules by means of density-functional and transition-potential theory, Phys. Rev. B 58 (1998) 8097–8110.

[9] M. Stener, G. Fronzoni, M. de Simone, Time dependent density functional theory of core electrons excitations, Chem. Phys. Lett. 373 (2003) 115 – 123.

[10] N. A. Besley, M. J. G. Peach, D. J. Tozer, Time-dependent density functional theory calculations of near-edge x-ray absorption fine structure with short-range corrected functionals, Phys. Chem. Chem. Phys. 11 (2009) 10350–10358.

[11] N. A. Besley, Fast time-dependent density functional theory calculations of the x-ray absorption spectroscopy of large systems, J. Chem. Theory Comput. 12 (2016) 5018–5025.

[12] N. A. Besley, Equation of motion coupled cluster theory calculations of the

X-ray emission spectroscopy of water, Chem. Phys. Lett. 542 (2012) 42 – 46.

[13] J. D. Wadey, N. A. Besley, Quantum chemical calculations of x-ray emission spectroscopy, J. Chem. Theory Comput. 10 (2014) 4557–4564.

[14] Y. Zhang, S. Mukamel, M. Khalil, N. Govind, Simulating valence-to-core X-ray emission spectroscopy of transition metal complexes with time-dependent density functional theory, J. Chem. Theory Comput. 11 (2015) 5804–5809.

[15] I. P. E. Roper, N. A. Besley, The effect of basis set and exchange-correlation functional on time-dependent density functional theory calculations within the Tamm-Dancoff approximation of the X-ray emission spectroscopy of transition metal complexes, J. Chem. Phys. 144 (2016) 114104.

[16] M. W. D. Hanson-Heine, M. W. George, N. A. Besley, Kohn-Sham density functional theory calculations of non-resonant and resonant X-ray emission spectroscopy, J. Chem. Phys. 146 (2017) 094106.

[17] J. S. Uejio, C. P. Schwartz, R. J. Saykally, D. Prendergast, Effects of vibrational motion on core-level spectra of prototype organic molecules, Chem. Phys. Lett. 467 (2008) 195 – 199.

[18] M. S. Dresselhaus, G. Dresselhaus, R. Saito, A. Jorio, Raman spectroscopy of carbon nanotubes, Phys. Rep. 409 (2005) 47.

[19] L. M. Malard, M. A. Pimenta, G. Dresselhaus, M. S. Dresselhaus, Raman spectroscopy in graphene, Physics Reports 473 (2009) 51–87.

[20] A. Jorio, M. A. Pimenta, A. G. S. Filho, R. Saito, G. Dresselhaus, M. S. Dresselhaus, Characterizing carbon nanotube samples with resonance raman scattering, New Journal of Physics 5 (2003) 139.

[21] Y. Miyauchi, S. Chiashi, Y. Murakami, Y. Hayashida, S. Maruyama, Fluorescence spectroscopy of single-walled carbon nanotubes synthesized from alcohol, Chem. Phys. Lett. 387 (2004) 198 – 203.

[22] X.-P. Tang, A. Kleinhammes, H. Shimoda, L. Fleming, K. Y. Bennoune, S. Sinha, C. Bower, O. Zhou, Y. Wu, Electronic structures of single-walled carbon nanotubes determined by NMR, Science 288 (2000) 492–494.

[23] C. Goze-Bac, S. Latil, P. Lauginie, V. Jourdain, J. Conard, L. Duclaux, A. Rubio, P. Bernier, Magnetic interactions in carbon nanostructures, Carbon 40 (2002) 1825 – 1842.

[24] E. Zurek, J. Autschbach, Density functional calculations of the 13C NMR chemical shifts in (9,0) single-walled carbon nanotubes, J. Am. Chem. Soc. 126 (2004) 13079–13088.

[25] N. A. Besley, J. J. Titman, M. D. Wright, Theoretical study of the 13C NMR spectroscopy of single-walled carbon nanotubes, J. Am. Chem. Soc. 127 (2005) 17948–17953.

[26] M. Aydin, D. L. Akins, Calculated dependence of vibrational band frequencies of single-walled and double-walled carbon nanotubes on diameter, Vibrational Spectroscopy 53 (2010) 163 – 172.

[27] T. Kupka, M. Stachów, E. Chełmecka, K. Pasterny, M. Stobińska, L. Stobiński, J. Kaminský, Efficient modeling of NMR parameters in carbon nanosystems, J. Chem. Theory Comput. 9 (2013) 4275–4286.

[28] W. A. Saidi, P. Norman, Probing single-walled carbon nanotube defect chemistry using resonance raman spectroscopy, Carbon 67 (2014) 17 – 26.

[29] P. R. Nagy, J. Koltai, P. R. Surjàn, J. Kürti, A. Szabados, Resonance raman optical activity of single walled chiral carbon nanotubes, J. Phys. Chem. A 120 (2016) 5527–5538.

[30] P. M. Tailor, R. J. Wheatley, N. A. Besley, An empirical force field for the simulation of the vibrational spectroscopy of carbon nanomaterials, Carbon 113 (2017) 299 – 308.

[31] J. A. Teprovich, A. L. Washington, J. Dixon, P. A. Ward, J. H. Christian, B. Peters, J. Zhou, S. Giri, D. N. Sharp, J. A. Velten, R. N. Compton, P. Jena, R. Zidan, Investigation of hydrogen induced fluorescence in C60 and its potential use in luminescence down shifting applications, Nanoscale 8 (2016) 18760–18770.

[32] J. Kawai, M. Motoyama, C K-V X-ray-emission spectra of solid $C_{70}$ with comparison to $C_{60}$, Phys. Rev. B 47 (1993) 12988–12991.

[33] A. A. El-Barbary, S. Trasobares, C. P. Ewels, O. Stephan, A. V. Okotrub, L. G. Bulusheva, C. J. Fall, M. I. Heggie, Electron spectroscopy of carbon materials: experiment and theory, J. Phys.: Conference Series 26 (2006) 149.

[34] B. Gao, L. Liu, C. Wang, Z. Wu, Y. Luo, Spectral identification of fullerene $C_{82}$ isomers, J. Chem. Phys. 127 (2007) 164314.

[35] T. Käämbre, J. Schiessling, L. Kjeldgaard, L. Qian, I. Marenne, J. N. O'Shea, J. Schnadt, D. Nordlund, C. J. Glover, J.-E. Rubensson, P. Rudolf, N. Mårtensson, J. Nordgren, P. A. Brühwiler, Bulk electronic structure of $K_3C_{60}$ as revealed by soft X-rays, Phys. Rev. B 75 (2007) 195432.

[36] A. V. Okotrub, L. G. Bulusheva, I. P. Asanov, A. S. Lobach, Y. M. Shulga, X-ray spectroscopic and quantum-chemical characterization of hydrofullerene $C_{60}H_{36}$, J. Phys. Chem. A 103 (1999) 716–720.

[37] Y. V. Lavskaya, A. V. Okotrub, L. G. Bulusheva, E. M. Pazhetnov, A. I. Boronin, N. I. Denisenko, O. V. Boltalina, X-ray emission and X-ray photoelectron spectroscopic studies of fullerene fluoride $C_{60}F_{24}$, Phys. Sol. State 49 (2007) 1195–1200.

[38] J. Guo, P. Skytt, N. Wassdahl, J. Nordgren, Y. Luo, O. Vahtras, H. gren, Resonant and non-resonant X-ray scattering from $C_{70}$, Chem. Phys. Lett. 235 (1995) 152 – 159.

[39] Käämbre, T., Qian, L., Rubensson, J.-E., Guo, J.-H., Sathe, C., Nordgren, J., Palmqvist, J.-P., Jansson, U., Study of oxygen-$C_{60}$ compound formation by NEXAFS and RIXS, Eur. Phys. J. D 16 (2001) 357–360.

[40] A. V. Okotrub, L. G. Bulusheva, D. Tomanek, X-ray spectroscopic and quantum chemical study of carbon tubes produced in arc-discharge, Chem. Phys. Lett. 289 (1998) 341 – 349.

[41] Y. V. Zaulichnyi, Y. M. Solonin, S. S. Zvezda, E. V. Prilutskii, O. V. Prilutskii, E. A. Kats, Features of the fine structure of the X-ray CK $\alpha$ emission bands of multiwalled carbon nanotubes, Powder Metallurgy and Metal Ceramics 45 (2006) 283–288.

[42] A. V. Okotrub, V. V. Belavin, L. G. Bulusheva, A. V. Gusel'nikov, A. G. Kudashov, D. V. Vyalikh, S. L. Molodtsov, Determination of the texture of arrays of aligned carbon nanotubes from the angular dependence of the x-ray emission and x-ray absorption spectra, J. Exp. Theor. Phys. 107 (2008) 517–525.

[43] J. Zhong, J. Chiou, C. Dong, L. Song, C. Liu, S. Xie, H. Cheng, W.-F. Pong, C. Chang, Y. Chen, Z. Wu, J. Guo, Probing quantum confinement of single-walled carbon nanotubes by resonant soft-X-ray emission spectroscopy, App. Phys. Lett. 93 (2008) 023107.

[44] P. J. Stephens, F. J. Devlin, C. F. Chabalowski, M. J. Frisch, Ab initio calculation of vibrational absorption and circular dichroism spectra using density functional force fields, J. Phys. Chem. 98 (1994) 11623–11627.

[45] P. C. Hariharan, J. A. Pople, The influence of polarization functions on molecular orbital hydrogenation energies, Theoret. Chim. Acta 28 (1973) 213–222.

[46] Y. Shao, Z. Gan, E. Epifanovsky, A. T. B. Gilbert, M. Wormit, J. Kussmann, A. W. Lange, A. Behn, J. Deng, X. Feng, D. Ghosh, M. Goldey, P. R. Horn, L. D. Jacobson, I. Kaliman, R. Z. Khaliullin, T. Ku, A. Landau,

J. Liu, E. I. Proynov, Y. M. Rhee, R. M. Richard, M. A. Rohrdanz, R. P. Steele, E. J. Sundstrom, H. L. W. III, P. M. Zimmerman, D. Zuev, B. Albrecht, E. Alguire, B. Austin, G. J. O. Beran, Y. A. Bernard, E. Berquist, K. Brandhorst, K. B. Bravaya, S. T. Brown, D. Casanova, C.-M. Chang, Y. Chen, S. H. Chien, K. D. Closser, D. L. Crittenden, M. Diedenhofen, R. A. D. Jr., H. Do, A. D. Dutoi, R. G. Edgar, S. Fatehi, L. Fusti-Molnar, A. Ghysels, A. Golubeva-Zadorozhnaya, J. Gomes, M. W. Hanson-Heine, P. H. Harbach, A. W. Hauser, E. G. Hohenstein, Z. C. Holden, T.-C. Jagau, H. Ji, B. Kaduk, K. Khistyaev, J. Kim, J. Kim, R. A. King, P. Klunzinger, D. Kosenkov, T. Kowalczyk, C. M. Krauter, K. U. Lao, A. D. Laurent, K. V. Lawler, S. V. Levchenko, C. Y. Lin, F. Liu, E. Livshits, R. C. Lochan, A. Luenser, P. Manohar, S. F. Manzer, S.-P. Mao, N. Mardirossian, A. V. Marenich, S. A. Maurer, N. J. Mayhall, E. Neuscamman, C. M. Oana, R. Olivares-Amaya, D. P. ONeill, J. A. Parkhill, T. M. Perrine, R. Peverati, A. Prociuk, D. R. Rehn, E. Rosta, N. J. Russ, S. M. Sharada, S. Sharma, D. W. Small, A. Sodt, T. Stein, D. Stck, Y.-C. Su, A. J. Thom, T. Tsuchimochi, V. Vanovschi, L. Vogt, O. Vydrov, T. Wang, M. A. Watson, J. Wenzel, A. White, C. F. Williams, J. Yang, S. Yeganeh, S. R. Yost, Z.-Q. You, I. Y. Zhang, X. Zhang, Y. Zhao, B. R. Brooks, G. K. Chan, D. M. Chipman, C. J. Cramer, W. A. G. III, M. S. Gordon, W. J. Hehre, A. Klamt, H. F. S. III, M. W. Schmidt, C. D. Sherrill, D. G. Truhlar, A. Warshel, X. Xu, A. Aspuru-Guzik, R. Baer, A. T. Bell, N. A. Besley, J.-D. Chai, A. Dreuw, B. D. Dunietz, T. R. Furlani, S. R. Gwaltney, C.-P. Hsu, Y. Jung, J. Kong, D. S. Lambrecht, W. Liang, C. Ochsenfeld, V. A. Rassolov, L. V. Slipchenko, J. E. Subotnik, T. V. Voorhis, J. M. Herbert, A. I. Krylov, P. M. Gill, M. Head-Gordon, Advances in molecular quantum chemistry contained in the Q-Chem 4 program package, Molecular Physics 113 (2015) 184–215.

[47] A. T. B. Gilbert, N. A. Besley, P. M. W. Gill, Self-consistent field calculations of excited states using the maximum overlap method (MOM), J.

Phys. Chem. A 112 (2008) 13164–13171.

[48] F. Gel'mukhanov, H. Ågren, Resonant inelastic x-ray scattering with symmetry-selective excitation, Phys. Rev. A 49 (1994) 4378–4389.

[49] Y. Luo, H. Ågren, F. Gel'mukhanov, Polarization anisotropy in resonant x-ray emission from molecules, Phys. Rev. A 53 (1996) 1340–1348.